Journal of Solid State Chemistry 187 (2012) 258–263

Contents lists available at SciVerse ScienceDirect

Journal of Solid State Chemistry

journal homepage: www.elsevier.com/locate/jssc

Substitutions into the trigonal bipyramidal site of $InGaCuO_4$

Rosa Grajczyk, Krishnendu Biswas, Romain Berthelot, Jun Li, A.W. Sleight, M.A. Subramanian *

Department of Chemistry, Oregon State University, Corvallis, OR 97331, USA

ARTICLE INFO

Article history:
Received 25 October 2011
Received in revised form
7 January 2012
Accepted 9 January 2012
Available online 24 January 2012

Keywords:
Transition metal oxides
Trigonal bipyramidal coordination
Dielectric properties
Magnetic properties

ABSTRACT

Solid solutions of $InMCu_{1-x}Mg_xO_4$ ($M=Ga^{3+}$, Al^{3+}) have been synthesized to understand the influence of the trigonal bipyramidal (TBP) crystallographic M^{3+}/Cu^{2+} site of the $YbFe_2O_4$-type structure through powder X-ray and neutron diffraction, dielectric and magnetism measurements. The addition of Mg^{2+} in the $InGaCuO_4$ lattice results in a decrease of the dielectric constant, but the dielectric loss is not affected until the concentration of Mg^{2+} is above $x=0.50$. The shift in the diffraction peaks, and subsequently the change in the lattice parameters, cannot be exclusively explained by the change in ionic radii. These results show the first observation of the reduction in axial bond lengths for TBP Cu^{2+} in a $YbFe_2O_4$-type crystal lattice.

1. Introduction

Oxides adopting the $YbFe_2O_4$-type crystal structure (space group $R\bar{3}m$) have been extensively studied as they exhibit remarkable structure-property relationships, in particular their multiferroic behavior. The mixed-valency of iron in $YbFe_2O_4$ was found to produce ferrimagnetic ordering below 250 K and ferroelectric ordering below 330 K [1,2]. The polarizability of the $LuFe_2O_4$ analog is known to be a result of the electron transfer between the Fe^{3+} and Fe^{2+} ions, [3] but the electronic conductivity of the samples produced an increase in the dielectric loss. High resistivity throughout the lattice, with regions of polarizability, would be expected to produce a large dielectric constant and decreased dielectric loss of the material [2].

$InM^{3+}M^{2+}O_4$ ($M^{3+}=Ga^{3+}$, Al^{3+} and $M^{2+}=Cu^{2+}$, Mg^{2+}) compounds are isostructural to $YbFe_2O_4$. Their structure is described a stacking of one InO_2 layer, made up of edge-sharing InO_6 octahedra, and a double layer of MO_5 edge-sharing trigonal bipyramids with disordered M^{2+} and M^{3+} cations (Fig. 1) [4–7]. The insulating behavior of $InGaCuO_4$ and $InAlCuO_4$, in addition to the polarizability of the d^9 cation Cu^{2+} in the TBP site, could lead to a successful dielectric material. Previous studies have found that the dielectric constant of $InGaCuO_4$ is lower than other $LnFe_2O_4$ compound analogs, and it was observed that both the dielectric constant and dielectric loss are highly frequency dependent above 220 K [1,2,8]. Regardless of the decreased dielectric constant, the addition of an insulating cation that does not have d electrons, such as Mg^{2+}, could reduce the observed dielectric loss [2].

In this paper, the influence of the d_z^2 orbital in the TBP site of $InGaCuO_4$ has been studied. The initial solid solution of $InGaCu_{1-x}Mg_xO_4$ showed a change in the lattice parameters that could not unequivocally be explained by a change in the ionic radii, which was determined to be a result of the electronic configuration of the Cu^{2+} in the TBP site (Fig. 2).

2. Experimental

2.1. Synthesis and phase analysis

Polycrystalline samples of $InGaCu_{1-x}Mg_xO_4$ ($x=0$–1) and $InAlCu_{1-x}Mg_xO_4$ ($x=0$–1) were prepared using standard solid state reactions. Stoichiometric amounts of each oxide were intimately mixed with ethanol, pelletized, and then heated at 1150 °C for 12–48 h with intermediate grindings. Each sample was analyzed for phase purity with a RIGAKU MINIFLEX II diffractometer over 5–60° 2θ using Cu K_α radiation and a graphite monochromator on the diffracted beam. Lattice parameters were refined using the GSAS software and EXPGUI user interface [9,10]. For the compound $InGaCu_{0.6}Mg_{0.4}O_4$, time-of-flight (TOF) powder neutron diffraction data was collected using the POWGEN (BL – 11A) neutron powder diffractometer at the Spallation Neutron Source at Oak Ridge National Laboratory, Oak Ridge, TN [11]. A 2.67 g sample was contained in a 8 mm diameter vanadium sample can and analyzed at room temperature over a d – spacing range of 0.317–6.164 Å. Rietveld refinements of the data employed the GSAS software and EXPGUI interface [9,10].

* Corresponding author.
E-mail addresses: rabinovr@onid.orst.edu (R. Grajczyk), krismat79@gmail.com (K. Biswas), berthelr@science.oregonstate.edu (R. Berthelot), jli100@yahoo.com (J. Li), arthur.sleight@oregonstate.edu (A.W. Sleight), mas.subramanian@oregonstate.edu (M.A. Subramanian).

0022-4596/$ - see front matter © 2012 Elsevier Inc. All rights reserved.
doi:10.1016/j.jssc.2012.01.026

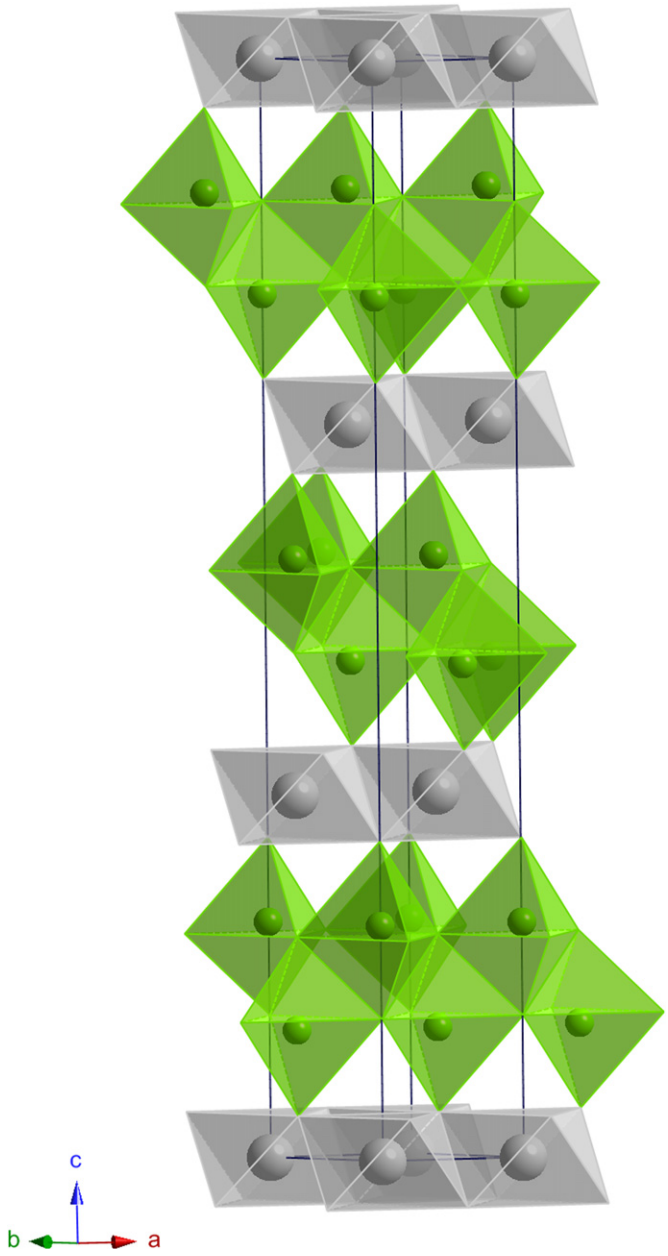

Fig. 1. Crystal structure of $InGaCuO_4$, with InO_6 octahedra (grey) and a double layer of MO_5 trigonal bipyramids (green). There is an equal distribution of M ions in the trigonal bipyramidal site [2].

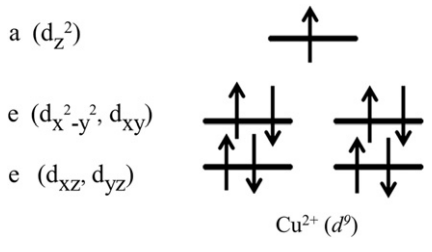

Fig. 2. Crystal field diagram of the *d* orbitals for Cu^{2+} (d^9).

The TOF peak-profile function number 3 (a convolution of back-to-back exponentials with a pseudo-Voigt) and the shifted Chebyschev function were used to model the diffraction peak profiles and backgrounds, respectively.

2.2. Dielectric and magnetism characterization

The dielectric properties of each sample were measured with an HP Precision LCR Meter 4284A (1 kHz to 1 MHz) over a temperature range of 35–180 °C. In order to increase the density of the pellets, which is necessary for optimum dielectric measurements, the samples were ball-milled for 6 h per intermediate grinding. The ball-milled samples were then sintered at 1150 °C for 6 h and coated with silver electrodes for the dielectric measurements. Zero field cooled (ZFC) DC magnetism data were collected with a Quantum Design Physical Properties Measurement System (PPMS) using the ACMS mode with a magnetic field of 0.50 T from 5 to 300 K.

3. Results and discussion

3.1. The $InGaCu_{1-x}Mg_xO_4$ solid solution

XRD patterns provided in Fig. 3 show single phase samples of $InGaCu_{1-x}Mg_xO_4$ were successfully produced for Mg content up to $x=0.80$. Our attempts to reproduce the synthesis of $InGaMgO_4$ reported by Moriga et al. [7] were unsuccessful. For compositions with $x \geq 0.70$, with the exception of $x=0.80$, a minor spinel phase of $MgGa_2O_4$ was observed, which could not be eliminated by further thermal treatments or employing a higher synthesis temperature.

The XRD patterns indicate a general shifting of the (00*l*) diffraction peaks, and Le Bail refinements demonstrate that both the *a* and the *c* cell parameters follow a linear trend with increasing Mg^{2+} content (Fig. 4). The *c*/*a* ratio also follows a linear trend, which is anticipated for a solid solution. A Rietveld refinement was completed for $InGaCu_{0.60}Mg_{0.40}O_4$ in the $R\bar{3}m$ space group starting from the parameters reported for $InGaCuO_4$ (Fig. 5) [9,10]. The In and O sites were fully occupied. The M site was constrained to be fully occupied with 50% occupation by Ga^{3+}. The bond angles of the TBP site deviated slightly from ideal values giving an umbrella-type arrangement, which is in agreement with the Type II TBP classification [12]. The distorted TBP site is shown in Fig. 6, where the cation in each TBP layer is off set from the basal plane producing one axial bond length to be longer

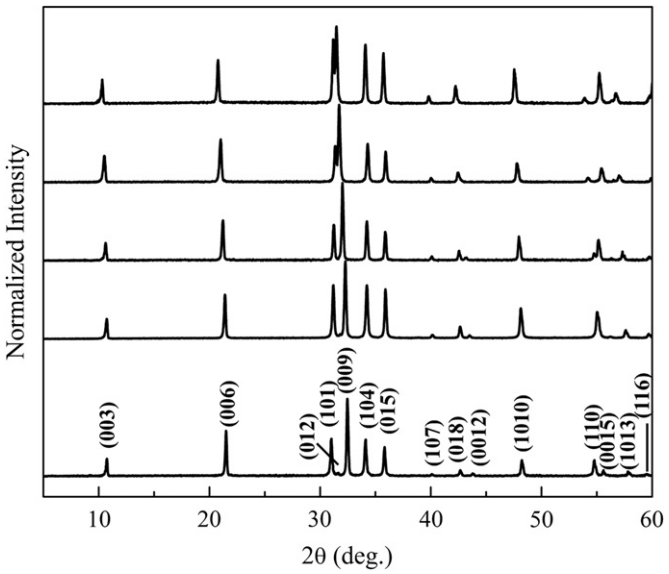

Fig. 3. XRD patterns of selected $InGaCu_{1-x}Mg_xO_4$, from bottom: $x=0$, 0.20, 0.40, 0.60, 0.80. A systematic shift to lower 2θ was observed for each reflection as the magnesium content was increased.

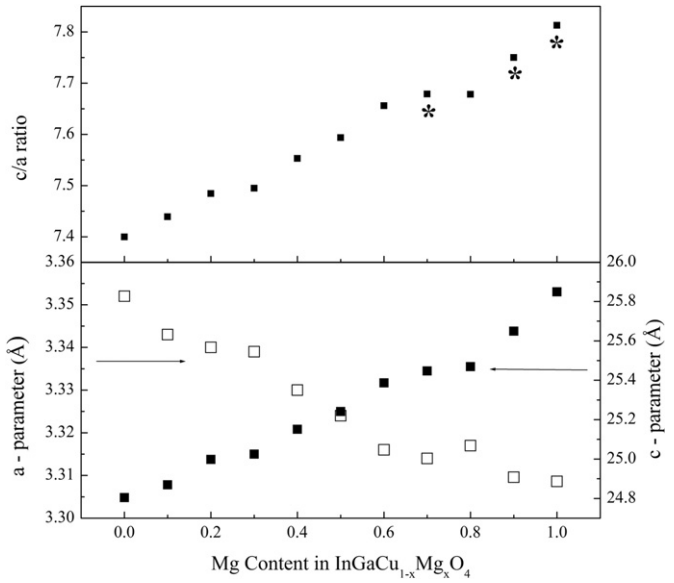

Fig. 4. (Top panel) The calculated c/a ratio shows a linear trend that is expected for a solid solution. (Bottom panel) Le Bail lattice refinement of the a and c axis for polycrystalline samples. The increase of the c parameter and the decrease of the a parameter is a result of the decrease in axial bond length reduction with the Mg^{2+} substitution into the $InGaCuO_4$ lattice. Asterisks indicate multiphase refinements where In_2O_3 and $MgGa_2O_4$ were present.

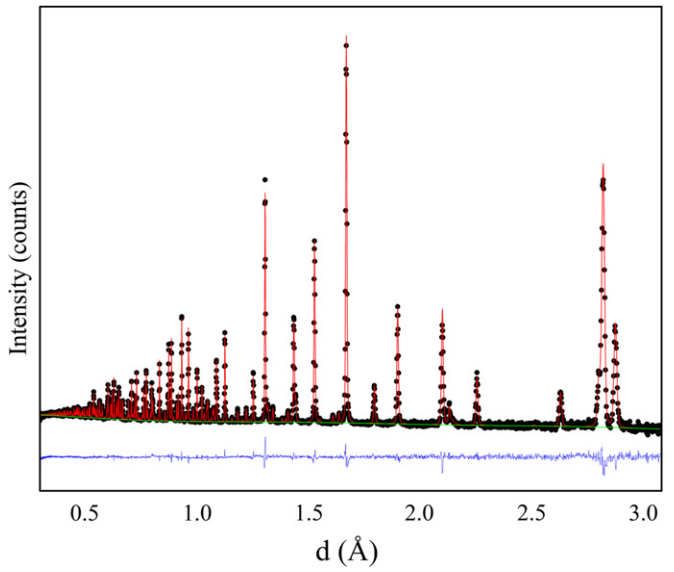

Fig. 5. Neutron diffraction pattern of $InGaCu_{0.60}Mg_{0.40}O_4$ where the observed intensity (black circle), calculated intensity (red line), background refinement (green line) and the difference calculation (blue line) are provided. The refinement verified that the nominal composition was correct and that the sample had full oxygen occupancy. (For interpretation of the references to color in this figure legend, the reader is referred to the web version of this article.)

than the other. The structural and geometric parameters are provided in Tables 1 and 2.

As a result of ball-milling, all of the samples were above 75% of theoretical density with the exception of one composition that had a density of 66% ($InGaCu_{0.20}Mg_{0.80}O_4$). The dielectric properties of $InGaCu_{1-x}Mg_xO_4$ have been examined and a selection of the data is provided in Fig. 7. The dielectric loss of these samples follows a relaxor behavior with values similar to what is reported in the literature and the dielectric constant is comparable to the reported values at room temperature [2,8]. Throughout the solid solution it can be seen that the dielectric constant is dependent

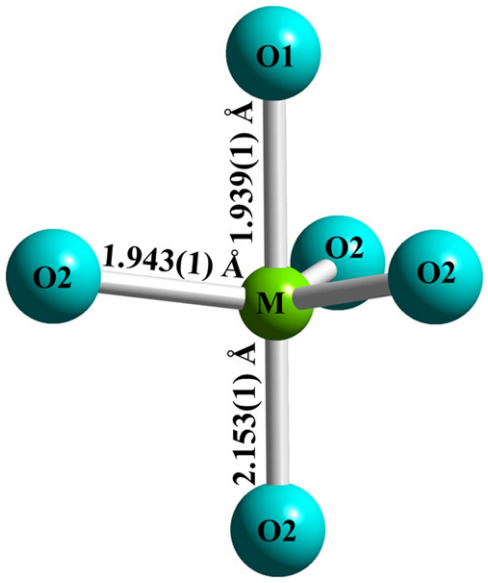

Fig. 6. Image of the TBP environment in $InGaCuO_4$, atomic labels provided for the bond distances and angles in Table 2.

Table 1
TOF neutron diffraction structure refinement[1] of $InGaCu_{0.60}Mg_{0.40}O_4$.

	In	M	O1	O2
Z	0	0.2148(1)	0.2918(1)	0.1292(1)
U_{iso} (Å^2)	0.63(1)	0.67(1)	0.65(1)	1.60(1)
U_{11} (Å^2)	0.38(3)	0.61(1)	0.70(1)	1.62(3)
U_{33} (Å^2)	1.15(4)	0.78(2)	0.59(3)	1.52(3)
U_{12} (Å^2)	0.19(2)	0.30(1)	0.35(1)	0.81(1)
Occupancy	0.98(1)	1[2]	1	1

1. Structure refinement completed in $R\bar{3}\ m$ space group, a=3.3342(1) Å, c=25.151(1) Å, R_{wp}=2.56%, R_p=4.43%, χ^2=2.901.
2. Based on an occupancy of Ga fixed at 0.50, the occupancies of Cu and Mg refine to 0.25(1), and 0.25(1), respectively.
3. Thermal parameters (U) were multiplied by 100, $U_{11}=U_{22}$, $U_{13}=U_{23}=0$.

Table 2
Bond lengths (Å) and angles (°).

$InGaCu_{0.60}Mg_{0.40}O_4$	
In – O1 (× 6)	2.190(1)
M – O1	1.939(1)
M – O2	2.153(1)
M – O2 (× 3)	1.943(1)
O1 – In – O1	99.17(1)
O1 – In – O1	80.83(1)
O1 – M – O2	97.88(1)
O2 – M – O2	82.12(1)
O2 – M – O2	118.15(1)

on temperature, frequency, and the concentration of Mg^{2+} in the sample. A comparison of the dielectric constant throughout the solid solution shows a change in the temperature dependence with increasing amounts of magnesium. Additionally, the dielectric loss of the solid solution becomes much more temperature dependent as the concentration of Mg^{2+} is increased.

The frequency dependence of $InGaCu_{1-x}Mg_xO_4$ illustrates that, as expected, the dielectric constant decreases as the applied

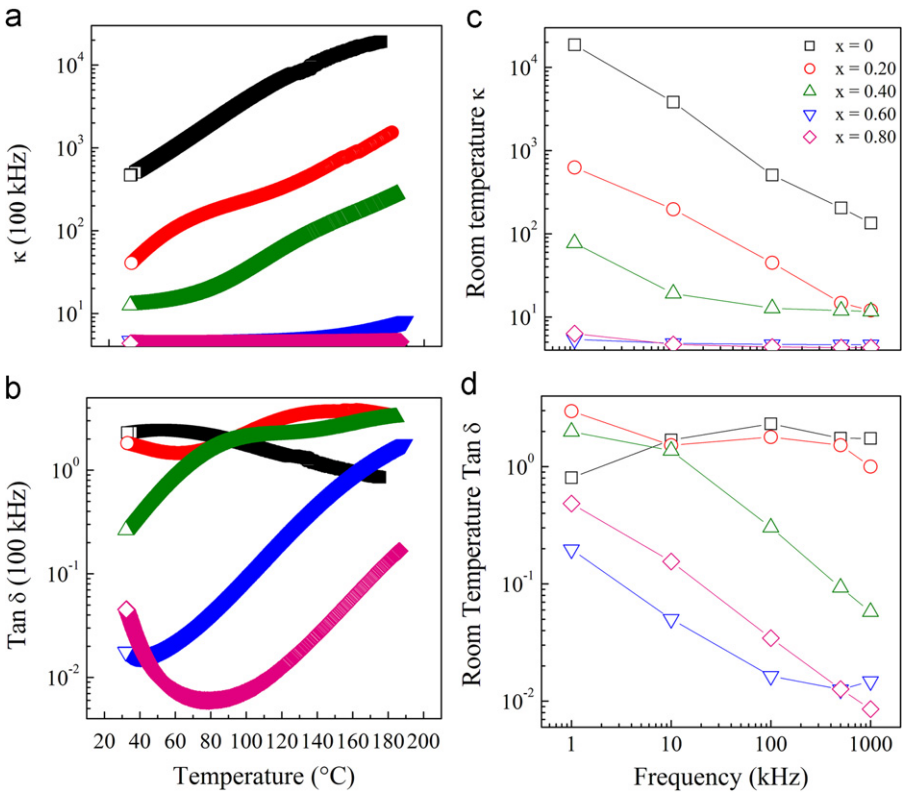

Fig. 7. (a) Temperature dependence of the dielectric constant (κ) for $InGaCuO_4$ (black square), $InGaCu_{0.80}Mg_{0.20}O_4$ (red circle), $InGaCu_{0.60}Mg_{0.40}O_4$ (green triangle), $InGaCu_{0.40}Mg_{0.60}O_4$ (blue inverse triangle) and $InGaCu_{0.20}Mg_{0.80}O_4$ (pink diamond) with the (b) dielectric loss ($\tan\delta$) at 100 kHz. (c) Frequency dependence of $InGaCu_{1-x}Mg_xO_4$ dielectric constant (d) and dielectric loss. The addition of the insulating Mg^{2+} ion decreases the polarizability of the material, which is apparent in both the temperature and frequency dependent plots. (For interpretation of the references to color in this figure legend, the reader is referred to the web version of this article.)

Table 3
Magnetic parameters of $InGaCu_{1-x}Mg_xO_4$[a].

x	θ	μ_{eff} (obs.)	μ_{eff} (calc.)
0	−35.107	1.849	1.73
0.1	−40.28	1.794	1.64
0.2	−46.136	1.688	1.55
0.3	−22.269	1.526	1.45
0.4	−10.084	1.395	1.34
0.5	−0.51	1.154	1.22
0.6	−3.642	0.996	1.09
0.8	−6.956	0.945	0.77

[a] All $1/\chi$ plots were fit using a temperature range of 100–300 K.

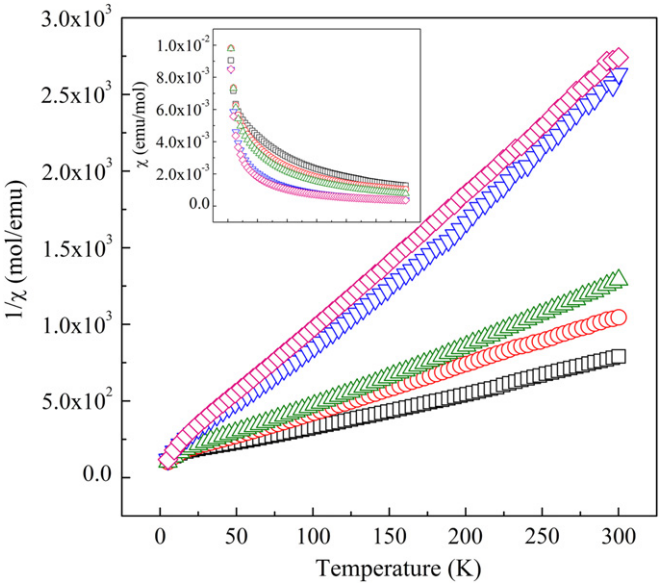

Fig. 8. Diamagnetic core corrected magnetism data for $InGaCu_{1-x}Mg_xO_4$: $x=0$ (black square), $x=0.20$ (red circle), $x=0.40$ (green triangle), $x=0.60$ (blue inverse triangle), and $x=0.80$ (pink diamond). The $1/\chi$ plot shows that there is no magnetic transition over the recorded temperature range. The magnetization of the Cu^{2+} d^9 electron is diluted as the concentration of Mg^{2+} increases, which is seen in the inset by a decrease in the observed χ.

frequency is increased (Fig. 7(c), and (d)). The decrease in frequency dependence throughout the solid solution is directly related to the increase in the insulating behavior of $InGaCuO_4$ when Mg^{2+} is added. The dielectric response of the compound can be described as the electronic polarizability given from the lone electron in the Cu^{2+} d_z^2 orbital. An increase in the concentration of Mg^{2+} dilutes the polarizability of the lattice, which restricts the electron polarizability to limited regions of the lattice.

The magnetic properties of $InGaCu_{1-x}Mg_xO_4$ are provided in Table 3, where all samples were corrected for core diamagnetization based on the values provided by Bain et al. (Fig. 8) [13]. It can be seen that although there is no observed magnetic ordering down to 5 K, the calculated Weiss constants indicate antiferromagnetic interactions for all compositions. The dilution of the Cu^{2+} is displayed through the trend on the magnetic moments, where the experimental spin values closely match those of the theoretical moments.

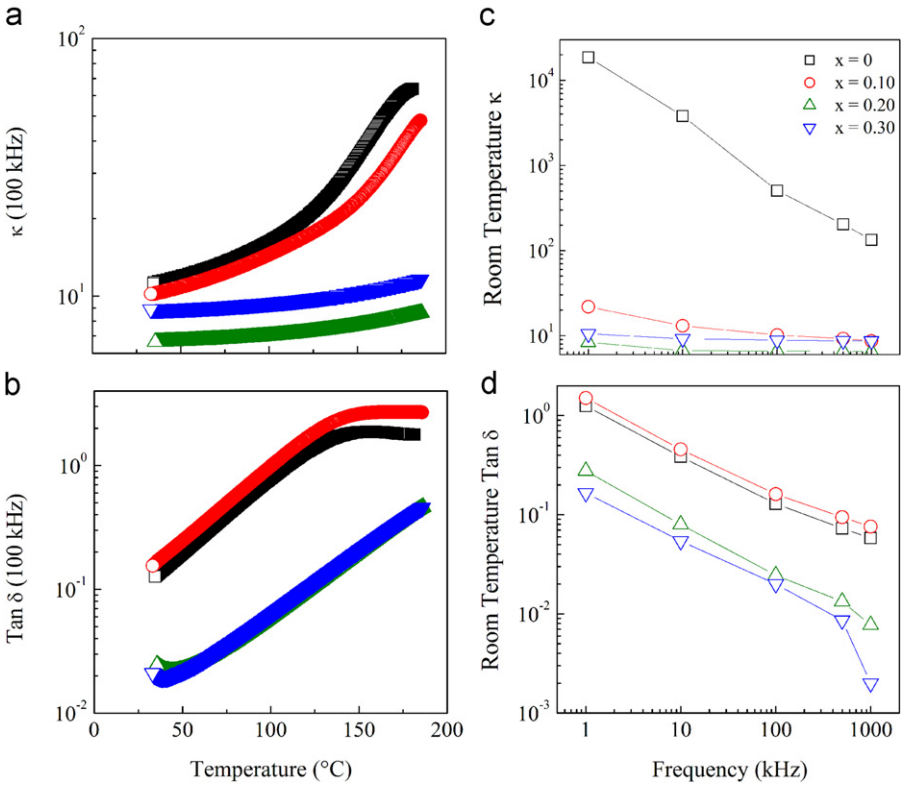

Fig. 9. (a) Temperature dependence of the dielectric constant (κ) for $InAlCuO_4$ (black square), $InAlCu_{0.90}Mg_{0.10}O_4$ (red circle), $InAlCu_{0.80}Mg_{0.20}O_4$ (blue inverse triangle) and $InAlCu_{0.70}Mg_{0.30}O_4$ (green triangle) with the (b) dielectric loss (tan δ) at 100 kHz. (c) Frequency dependence of $InAlCu_{1-x}Mg_xO_4$ dielectric constant (κ) and (d) dielectric loss (tan δ). The smaller ionic radii of Al^{3+} limits the polarizability of the material in comparison to the gallium system, decreasing the observed dielectric constant by orders of magnitude. (For interpretation of the references to color in this figure legend, the reader is referred to the web version of this article.)

3.2. The $InAlCu_{1-x}Mg_xO_4$ solid solution

Samples of $InAlCu_{1-x}Mg_xO_4$ were synthesized and then characterized under the same conditions as their gallium – content analogs. Single phase samples were produced for values of x= 0–0.30, and Le Bail refinements were completed to determine if a shift in the lattice parameters was apparent. Multiple attempts were made to produce samples of x=0.40–1, but after extensive thermal treatments and increased firing temperatures, phase pure samples were not achieved. Multiphase Le Bail refinements of these samples showed a shift in the lattice parameters that indicated a solid solution of the major $InAlCu_{1-x}Mg_xO_4$ phase, even though diffraction peaks from the starting materials were still observed (See Supporting Information).

The dielectric properties were analyzed for the limited number of single phase $InAlCu_{1-x}Mg_xO_4$ compositions. The dielectric constant of the $InAlCuO_4$ parent compound was found to be much lower than the $InGaCuO_4$ composition and additional Mg content further decreased this value. The temperature and frequency dependence of the $InAlCu_{1-x}Mg_xO_4$ samples show that a small amount of Mg^{2+} decreased the dielectric constant to an extremely low value (Fig. 9). The change in atomic size from Ga^{3+} to Al^{3+} could be the reason for this decreased amount of polarizability, leading to an ordering of the atoms in the TBP site. With a larger difference between the ionic radii for Al^{3+} and Cu^{2+} in the five-fold coordination, 0.48 Å and 0.65 Å, respectively, the atoms may become ordered and decrease the overall polarizability of the material [14].

3.3. Structural variations

The M–O distances we find for $InGaCu_{0.60}Mg_{0.40}O_4$ are compared with those reported for $InGaCuO_4$ and $InGaMgO_4$ in Table 4. The axial bond lengths increase with Mg^{2+} doping, and it is observed that one axial bond is much longer than the other. The increase in the axial bond lengths is coupled with a decrease of the three basal plane M–O distances. This difference between axial bond lengths within a TBP unit is characteristic of the $YbFe_2O_4$-type structure whereas this difference does not occur for the single layer analogs, such as $YMnO_3$. In the $YMnO_3$ structure all O atoms forming the axial M–O bonds are coordinated to only 1 M atom. This situation occurs for only one of the two axial bonds of the TBP unit in the case of the $YbFe_2O_4$-type structure. The O atom forming the other axial bond is also forming three strong M–O bonds in the basal plane of the TBP unit. This O atom has consumed most of its bonding power in these 3 bonds. Thus, the axial bond that it forms is much weaker and longer than the other axial bond. On substitution of Cu^{2+} into $InGaMgO_4$ it is apparent that the hole in the 3d shell of Cu^{2+} occurs in the $3d_z^2$ orbital causing shrinkage of the axial M–O bond lengths. The longer axial M–O bond distance decreases much more than the shorter axial M–O distance. The decrease of these axial M–O distances in turn causes a shrinkage of the c cell edge despite the increase in the a cell edge that occurs with increasing Cu^{2+} concentration. This shrinkage of the axial bond lengths is caused by a hole in the $3d_z^2$ orbital without reducing the symmetry.

Table 4
Axial bond lengths in $InGaCu_{0.60}Mg_{0.40}O_4$ and the end members of $InGaCu_{(1-x)}Mg_xO_4$ (Å).

	$InGaCuO_4$ [6]	$InGaCu_{0.60}Mg_{0.40}O_4$	$InGaMgO4$ [7]
M−O1	1.920	1.939(1)	1.948
M–O2	2.106	2.153(1)	2.289
M–O2 (× 3)	1.953	1.943(1)	1.932

4. Conclusion

The solid solution of $InGaCu_{1-x}Mg_xO_4$ was successfully produced for $x=0$–0.80, with slight $MgGa_2O_4$ impurities for $x=0.70$, 0.90 and 1. It was determined that the large increase in the c parameter from $InGaCuO_4$ to $InGaMgO_4$, approximately 4%, could not be attributed to the change in the ionic radii from Cu^{2+} to Mg^{2+}. Neutron diffraction was used to compare the axial bond lengths of the TBP site for $InGaCu_{0.60}Mg_{0.40}O_4$ and the end members of $InGaCu_{(1-x)}Mg_xO_4$. The hole in the d_z^2 orbital of d^9 Cu^{2+} causes a reduction in axial bond lengths of the TBP unit, which in turn causes the reduction in the c cell edge. On dilution of Cu^{2+} with Mg^{2+}, this reduction of axial bond lengths and the c cell edge disappears. At this time, further research is in progress with additional transition metal dopants to verify the influence of the d orbital occupancies.

Acknowledgments

This work was supported by NSF Grant DMR 0804167. We thank Ashfia Huq, Jason Hodges, and the additional instrument scientists for their assistance during the ORNL POWGEN Neutron Diffraction workshop. This research at Oak Ridge National Laboratory's Spallation Neutron Source was sponsored by the Scientific User Facilities Division, Office of Basic Energy Sciences, U.S. Department of Energy under contract DE-AC05-00OR22725 with UT Battelle, LLC.

Appendix A. Supplementary information

Supplementary data associated with this article can be found in the online version at doi:10.1016/j.jssc.2012.01.026.

References

[1] K. Yoshii, N. Ikeda, Y. Matsuo, Y. Horibe, S. Mori, Phys. Rev. B 76 (2007) 024423.
[2] K. Yoshii, N. Ikeda, Y. Okajima, Y. Yoneda, Y. Matsuo, Y. Horibe, S. Mori, Inorg. Chem. 47 (2008) 6493–6501.
[3] M.A. Subramanian, T. He, J. Chen, N.S. Rogado, T.G. Calvarese, A.W. Sleight, Adv. Mater. 18 (2006) 1737–1739.
[4] N. Kimizuka, T. Mohri, J. Solid State Chem. 60 (1985) 382–384.
[5] N. Kimizuka, T. Mohri, J. Solid State Chem. 78 (1989) 98–107.
[6] A. Roesler, D. Reinen, Z. Anorg. Allg. Chem. 479 (1981) 119–124.
[7] T. Moriga, T. Sakamoto, Y. Sato, A.H. Khalid@ Haris, R. Suenari, I. Nakabayashi, J. Solid State Chem. 142 (1999) 206–213.
[8] D.P. Cann, R. Martin, C. Taylor, N. Vittayakorn, Mater. Lett. 58 (2004) 2147–2151.
[9] A.C. Larson, R.B. Von Dreele, General Structure Analysis System (GSAS), Los Alamos National Laboratory Report LAUR 86-748, 1994.
[10] B.H. Toby, J. Appl. Cryst. 34 (2001) 210–213.
[11] A. Huq, J.P. Hodges, O. Gourdon, L. Heroux, Z. Kristallogr. Proc. 1 (2011) 127–135.
[12] M. Nespolo, M. Isobe, J. Iida, N. Kimizuka, Acta Crystallogr., B Struct. Sci. 56 (2000) 805–810.
[13] G. Bain, J. Berry, J. Chem. Educ. 85 (2008) 532–536.
[14] R.D. Shannon, Acta Cryst. A 32 (1976) 751–767.